

Article

Evolution of Primary and Eutectic Si Phase and Mechanical Properties of Al₂O₃/Al-20Si Composites under High Pressure

Xiaohong Wang ^{1,*} , Zhipeng Chen ^{1,2}, Tengfei Ma ¹, Dongdong Zhu ^{1,*}, Duo Dong ^{1,*}, Xiaohong Yang ³, Li Liu ¹ and Gang Wang ²

- ¹ Key Laboratory of Air-Driven Equipment Technology of Zhejiang Province, Quzhou University, Quzhou 324000, China; zhipeng1021@126.com (Z.C.); matengfeihit@163.com (T.M.); li_liull@163.com (L.L.)
- ² School of Mechanical and Automotive Engineering, Anhui Polytechnic University, Wuhu 241000, China; gangwang@ahpu.edu
- ³ School of Mechanical and Electrical Engineering, Jinhua Polytechnic, Jinhua 321017, China; jhyxh65@126.com
- * Correspondence: hitxiaohong_wang@hotmail.com (X.W.); zhudd8@163.com (D.Z.); dongduohit@163.com (D.D.); Tel.: +86-138-0461-0088 (D.Z.); +86-151-0570-3275 (D.D.)

Abstract: To further improve the mechanical properties of Al-Si alloys. The phase, microstructure and mechanical properties of Al₂O₃/Al-20Si composites under different pressures were studied. The results show that the phase of Al₂O₃/Al-20Si composites are composed of α -Al phase, β -Si phase and Al₂O₃. Under the condition of hot-pressing sintering (0.02 GPa), a large number of Si phases with irregular shape and sharp angle are distributed on the α -Al matrix. Under high pressure solidification, the growth of primary Si phase is inhibited and the eutectic Si is spheroidized obviously. The microhardness of Al₂O₃/Al-20Si composite increases from 102.5 HV_{0.05} at 0.02 GPa to 156.4 HV_{0.05} at 4 GPa, which increases by 52.6%. The compressive strength increased from 381.5 MPa at 0.02 GPa to 469.1 MPa at 4 GPa, increasing by 23%. With the increase of solidification pressure, the fracture mechanism changes from cleavage fracture to quasi cleavage fracture.

Keywords: composite; phase transformation; Si; microstructure; stress/strain relationship



Citation: Wang, X.; Chen, Z.; Ma, T.; Zhu, D.; Dong, D.; Yang, X.; Liu, L.; Wang, G. Evolution of Primary and Eutectic Si Phase and Mechanical Properties of Al₂O₃/Al-20Si Composites under High Pressure. *Crystals* **2021**, *11*, 364. <https://doi.org/10.3390/cryst11040364>

Academic Editors: Yijie Zhang, Zhifeng Zhang, Zhiming Shi, Anna Knaislova and Shujun Zhang

Received: 11 March 2021
Accepted: 26 March 2021
Published: 30 March 2021

Publisher's Note: MDPI stays neutral with regard to jurisdictional claims in published maps and institutional affiliations.



Copyright: © 2021 by the authors. Licensee MDPI, Basel, Switzerland. This article is an open access article distributed under the terms and conditions of the Creative Commons Attribution (CC BY) license (<https://creativecommons.org/licenses/by/4.0/>).

1. Introduction

High silicon (20–26%) aluminum alloy has the characteristics of low density, low thermal expansion coefficient, good wear resistance and excellent comprehensive mechanical properties, so it is often used as a matrix alloy in aerospace, automobile, ship, electronic packaging fields [1,2]. The high silicon aluminum alloy prepared by conventional solidification method is composed of primary Si and Al (Si) eutectic. The higher the silicon content, the better the wear resistance and heat resistance of Al-Si alloy, and the lower the coefficient of thermal expansion. However, due to the coarse size and irregular shape of primary phase Si, it is easy to be cracked during the process of service, and the stress concentration exists near the sharp angle, which becomes the source of cracks. After the stress is applied, the crack propagates and breaks, deteriorating the mechanical properties of the material [3,4]. Therefore, it is still of great significance to improve the comprehensive mechanical properties of high silicon aluminum alloy by changing the primary Si phase [5].

At present, researchers mainly improve the mechanical properties of Al-Si alloy by changing the morphology of primary Si or inhibiting the formation of primary Si based on chemical and physical methods [6]. Chemical methods usually use modifier to refine coarse silicon phase. There are many kinds of refinement modification technology, such as RE (Rheniumrodmmmdiameter), P (Phosphorus), Na (Sodium), P+RE (Phosphorus + Rheniumrodmmmdiameter) composite modifier.

The effects of P and RE contents on the microstructure and mechanical properties of hypereutectic Al-20Si alloy were studied by adding phosphorus and rare earth into hypereutectic Al-20Si alloy [7]. The results show that the effect of phosphorus is mainly to

refine primary silicon, and rare earth can refine both primary silicon and eutectic silicon, but the modification effect of rare earth element alone is not obvious. The effect of Nd on primary silicon and eutectic silicon in hypereutectic Al-20wt.% Si alloy was studied by Xu et al. [8]. The results show that Nd can not only modify eutectic silicon in hypereutectic Al-20wt.% alloy, but also modify primary silicon. Some researchers added Na to refine grains, but neither Na nor Na salt has long-term effect, and the modified eutectic silicon cannot exceed 20 μm [9].

In terms of physical methods, Wei Hongmei et al. [10] studied the solidification behavior of fiber reinforced Al-18Si composites by squeeze casting. The effects of squeeze casting parameters on the nucleation and growth of primary silicon in composite materials were studied. In addition, with the rapid cooling technology innovation. The Al-Si alloy prepared by rapid solidification technology usually has the size of primary Si near nanoscale [11]. This microstructure makes the material have excellent mechanical properties and wear resistance, and is easier to be processed. However, the implementation conditions of rapid cooling technology are limited and cannot be produced on a large scale. Tian et al. [12] prepared aluminum matrix composites by pressure infiltration method, mainly studied the optimal combination of temperature and infiltration pressure to homogenize and granulate primary silicon. In addition, researchers have tried to use semi-solid forming method to prepare fine and uniform Al-Si alloy [13–15], such as mechanical stirring method, low superheat and weak mechanical stirring method, ultrasonic vibration method, etc., but most of them are in the experimental research stage, and few of them have realized industrial application.

To sum up, neither chemical nor physical methods can fundamentally solve the problem of coarse primary silicon effectively. However, a large number of studies have been carried out on Al-Si composites reinforced by Al_2O_3 ceramic particles recently [16–18], which show that Al_2O_3 particles can effectively refine primary silicon and eutectic silicon. It can be attributed to the fact that the crystal structures of Si and Al_2O_3 are similar, and the lattice parameter mismatch degree of Si and Al_2O_3 is about 3% [19]. According to BRAMFITT B L [20], effective nucleation occurs when the lattice mismatch is less than 6%. Therefore, Al_2O_3 can be used as an effective nucleation substrate for primary silicon during solidification. However, according to Mihira Acharya's research, the addition of Al_2O_3 does not improve the properties of Al-20Si alloy that much.

Therefore, it is proposed to solve this problem by using high pressure solidification method. High pressure solidification is carried out under extreme high-pressure environment, the crystal nucleation rate is greatly improved, and the element diffusion is restrained, which affects the solute redistribution process [21–23]. Under the condition of ultra-high pressure, the melting point, density and element distribution coefficient of the material are also greatly changed [24], and some reactions which cannot be carried out under normal pressure will occur, so that the new phase will be formed, and finally the solidified microstructure will be changed, which will affect the properties of the material.

Ma pan et al. [25] studied the solidification microstructure of Al-20Si alloy under different pressures. The results show that primary Si phase exists after solidification at atmospheric pressure and 1 GPa but disappears at higher pressure. The primary α -Al phase begins to form at 2 GPa, and its amount increases with the increase of pressure. The microstructure of $\text{Mg}_{96.17}\text{Zn}_{3.15}\text{Y}_{0.50}\text{Zr}_{0.18}$ alloy solidified under high pressure of 2–6 GPa was studied by Lin, X. P. et al. [26]. The results show that the microstructure of the alloy is refined obviously with the increase of GPa high pressure. The second phase changes from lamellar eutectic network structure under atmospheric pressure to discontinuous fine rod or particle under 6 GPa. At 6 GPa, the compressive strength increased from 263 MPa to 437 MPa. Liu, X. et al. [27] studied the solidification of Al-xCu alloys containing $x = 15, 33$ and 40 wt% Cu at different pressures (atmospheric pressure, 1 GPa, 2 GPa and 3 GPa). The results show that the morphology of eutectic Al_2Cu phase in Al-15Cu alloy changes with the pressure. The secondary arm spacing of Al-33Cu alloy and the size of primary Al_2Cu in Al-40Cu alloy decrease due to high pressure.

Based on the introduction above, to further improve the strength of the Al-Si alloy, the addition of ceramic particles and the effect of high pressure are considered. In this project, the microstructure evolution, and mechanical properties of Al₂O₃/Al-20Si alloy under different pressures were studied, and the strengthening mechanism of the alloy under high pressure was obtained.

2. Materials and Methods

Al powder (99.9%, 80 μm), Si powder (99.9%, 80 μm) and α-Al₂O₃ particles (20 μm) were used to prepare Al₂O₃/Al-20Si composite powder (Al₂O₃ particles accounted for 10% of the total volume). Alcohol was added into the ball mill to mix the powder for 6 h, and the rotational speed was 200 r/min. The uniform powder was prepared by hydraulic press in the cold pressing die to obtain Φ 9.6 × 10 mm rod sample. Then, wrapped with insulation ring, sealed in pyrophyllite mold. The high-pressure experiment was carried out on Htds-032F six-anvil press. When the pressure reached the set value (3 and 4 GPa), the sample were heated to 1000 °C for 30 min and then cooled down to the room temperature. Finally, the high-pressure solidification sample was obtained. As the contrast sample, the sample was prepared by ZT-40-20Y vacuum hot pressing furnace with the pressure of 0.02 GPa. According to the phase diagram, the low temperature liquid phase sintering was adopted. The hot pressing sintering temperature was 750 °C, and the hot pressing sintering atmosphere was 99.99% argon. Before 550 °C, the temperature was raised at the heating rate of 10° /min, and the pressure was 20 MPa. After 550 °C, the temperature was raised at the speed of 5 °C/min, and the pressure kept as the same. The hot pressing sintering was carried out under a small pressure and kept at 750 °C for 1.5 h, In order to facilitate the demolding, a layer of Boron Nitride was coated on the graphite model before sintering.

The phase analysis was carried out by Brooke D8 advance X-ray diffractometer (XRD, Brooke/German) with scanning step of 0.4 and scanning angle of 20–80°. Hitachi SU8010 Scanning electron microscope (SEM, Hitachi/Japan) was used to analyze the microstructure and energy spectrum of the solidified samples under different pressures. The density of the materials was measured by Archimedes drainage method. The microhardness of the materials was measured by DUH-211S Shimadzu dynamic microhardness tester (Shimadzu/Japan). In order to improve the accuracy of the results, the average value of 5 times of results was taken. The samples were cut into 2 mm × 2 mm × 4 mm for strength measurement, and the compression rate was set as 0.5 mm/min (landmark 370.10).

3. Results

3.1. Microstructure of Al₂O₃/Al-20Si Composites

The phase composition of Al₂O₃/Al-20Si composite prepared under different pressure was analyzed by X-ray diffraction as can be seen in Figure 1. It shows that the Al₂O₃/Al-20Si composite consists of α-Al phase, β-Si phase and Al₂O₃ strengthening phase, and no new phase is produced during high pressure solidification. In addition, it can be found that the diffraction peak of α-Al phase is shifted to the higher angel compared with 0.02 GPa. According to Bragg equation and the lattice constant formula of the face center cubic, the lattice constant of α-Al decreases. From the atomic point of view, the radius of Al atom is slightly larger than that of Si atom. With the increase of solidification pressure, more Si atoms replace Al atoms in phase α-Al, which leads to the decrease of lattice constant, and eventually leads to the shift of diffraction peak of α phase to high angle.

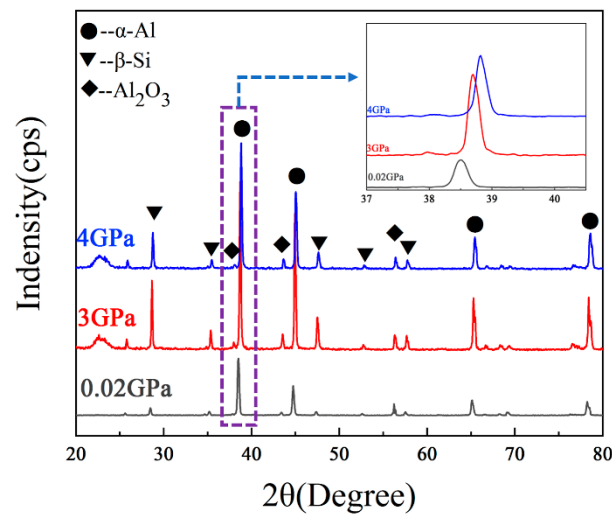


Figure 1. X-ray diffraction (XRD) pattern of $\text{Al}_2\text{O}_3/\text{Al-20Si}$ composite.

Figure 2 shows the microstructure of $\text{Al}_2\text{O}_3/\text{Al-20Si}$ composite under 0.02 GPa pressure. It can be seen that the $\text{Al}_2\text{O}_3/\text{Al-20Si}$ composite is mainly composed of gray white phase, agglomerated black phase, irregular bulk black phase and small white phase with dispersed distribution. The agglomerated black phase is distributed at the grain boundary. Table 1 shows the Electron Diffraction Spectrum (EDS) analysis results of matrix phase and black phase in $\text{Al}_2\text{O}_3/\text{Al-20Si}$ composite prepared under different conditions. The results show that the solid solubility of Si in the matrix phase of $\text{Al}_2\text{O}_3/\text{Al-20Si}$ composite prepared by 0.02 GPa is 1.94%. Therefore, the gray white matrix phase is $\alpha\text{-Al}$. The content of Si in the gray white bulk phase is 98.45%. Combined with the XRD results, the gray white massive phase is $\beta\text{-Si}$ phase. Then the white phase is Al_2O_3 . Compared with 0.02 GPa, the solid solubility of Si in α phase of $\text{Al}_2\text{O}_3/\text{Al-20Si}$ composite prepared by high pressure solidification is greatly increased. The solid solubility at 3 GPa and 4 GPa is 3.43% and 3.94%, respectively. Compared with 0.02 GPa, the solid solubility of Si increased by 103.1%.

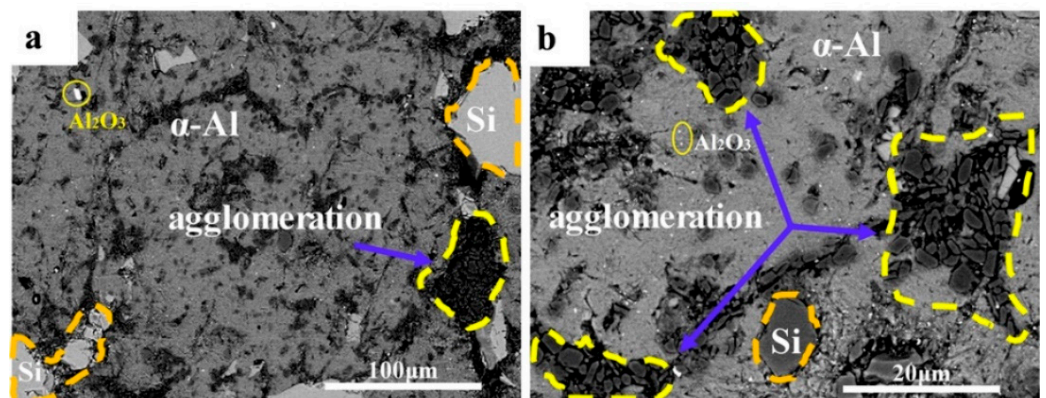


Figure 2. Scanning Electron Microscopy (SEM) microstructures of $\text{Al}_2\text{O}_3/\text{Al-20Si}$ composite under 0.02 GPa (a) 100 times, (b) 500 times.

Table 1. Electron Diffraction Spectrum (EDS) analysis of matrix phase and black phase of $\text{Al}_2\text{O}_3/\text{Al-20Si}$ composites.

Phase	0.02 GPa			3 GPa			4 GPa		
	Al (wt%)	Si (wt%)	O (wt%)	Al (wt%)	Si (wt%)	O (wt%)	Al (wt%)	Si (wt%)	O (wt%)
Matrix	98.06	1.94	0	96.57	3.43	0	96.06	3.94	0
Bulk grey phase	1.55	98.45	0	1.61	98.39	0	1.40	98.60	0
White phase	53.11	2.88	44.01	51.62	2.67	45.71	51.38	2.56	46.06

Figure 3 shows the microstructure of $\text{Al}_2\text{O}_3/\text{Al-20Si}$ composite prepared under different high pressures. It can be seen that the microstructure under 3 GPa is composed of black matrix phase α , spherical eutectic ($\alpha + \beta$) phase with network distribution at the grain boundary, and a small amount of Al_2O_3 strengthening phase with agglomerated distribution. There was no obvious change in the solidification microstructure at 4 GPa. However, the content of eutectic ($\alpha + \beta$) phase increased at the grain boundary, and the agglomeration of Al_2O_3 was greatly improved. Compared with Figure 2, the bulk primary β -Si phase disappears under high pressure, which indicates that the microstructure of $\text{Al}_2\text{O}_3/\text{Al-20Si}$ composite changes into hypoeutectic. It is because with the increase of solidification pressure, the eutectic point moves to the direction of silicon significantly, and the eutectic temperature also increases [28].

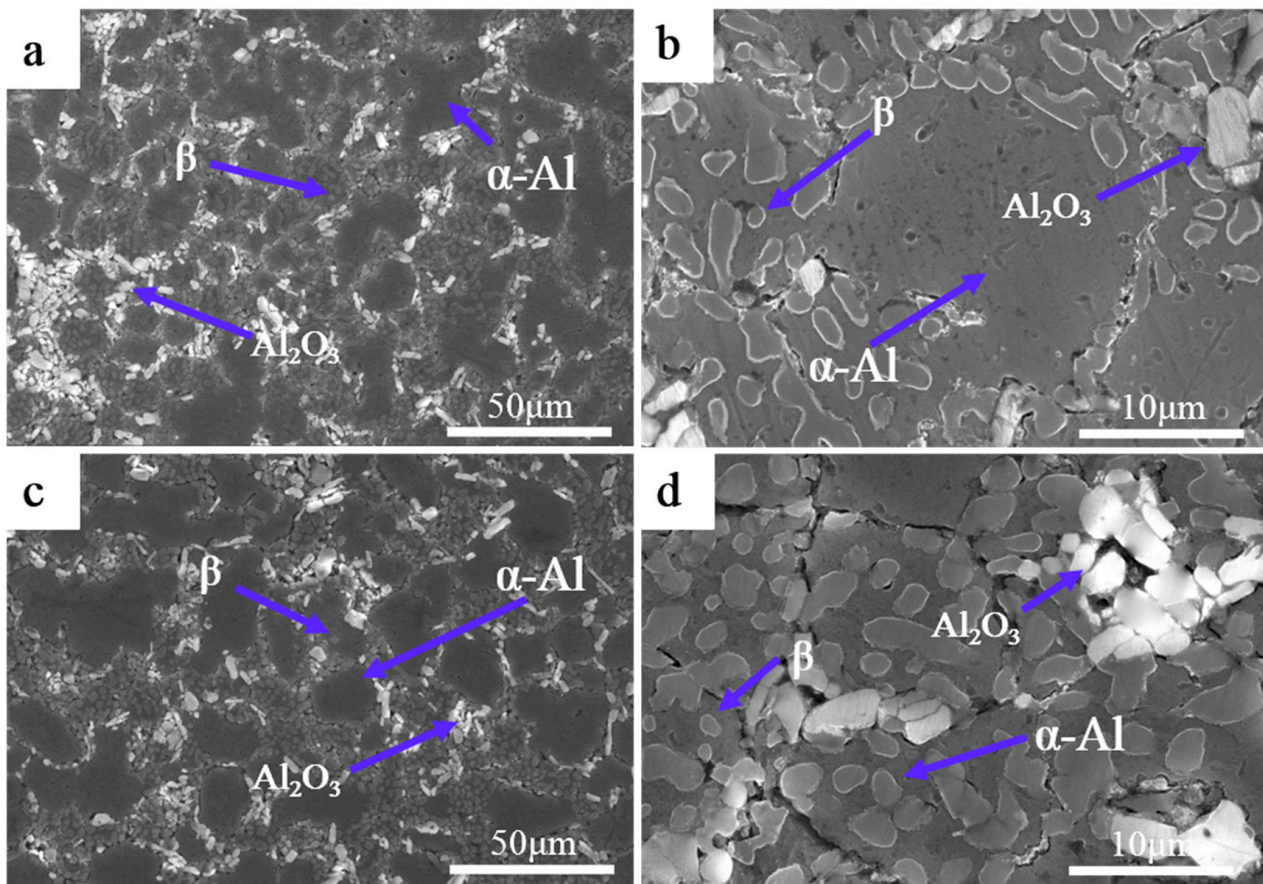


Figure 3. High-pressure solidified $\text{Al}_2\text{O}_3/\text{Al-20Si}$ composite morphology (a,b) 3 GPa, (c,d) 4 GPa.

Figure 4 shows the morphology of eutectic Si phase of $\text{Al}_2\text{O}_3/\text{Al-20Si}$ composites prepared by different methods. It is obviously found that the eutectic Si of the $\text{Al}_2\text{O}_3/\text{Al-20Si}$ composite prepared under the condition of 0.02 GPa is needle like or strip-shaped. The eutectic Si solidified at 3 GPa is in the shape of short rod. When the solidification pressure is further increased to 4 GPa, the size of eutectic Si is further reduced, and the shape is gradually spheroidized. The length-diameter ratio is close to 1.

The length diameter ratio of eutectic Si phase prepared under different pressures is counted, and the results are shown in Figure 5. It shows that the length diameter ratio of eutectic Si phase is 7.68 at 0.02 GPa. After high pressure solidification, eutectic silicon gradually spheroidized. When the solidification pressure is 3 GPa and 4 GPa, the length diameter ratio of eutectic Si decreases to 3.26 and 1.32, respectively. The results show that high pressure solidification can refine the eutectic Si grains of $\text{Al}_2\text{O}_3/\text{Al-20Si}$ composites.

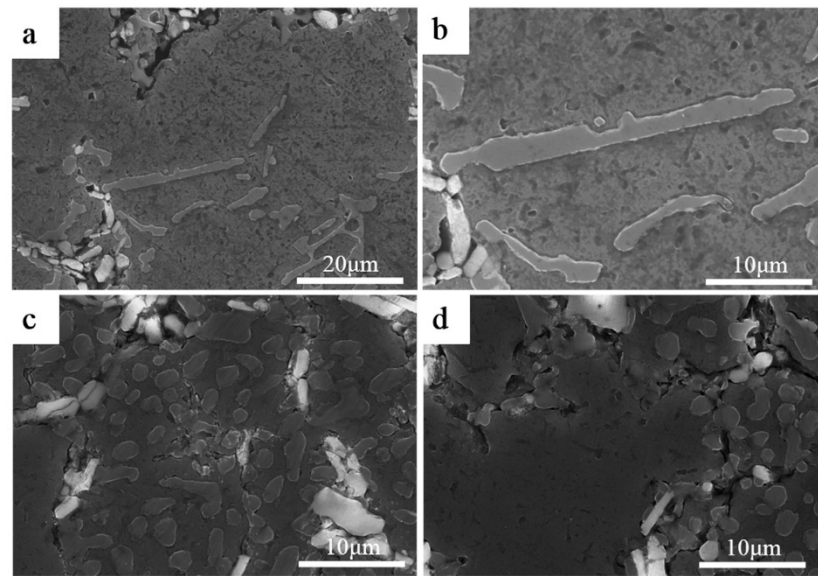


Figure 4. Al₂O₃/Al-20Si composite eutectic Si morphology (a,b) 0.02 GPa, (c) 3 GPa, (d) 4 GPa.

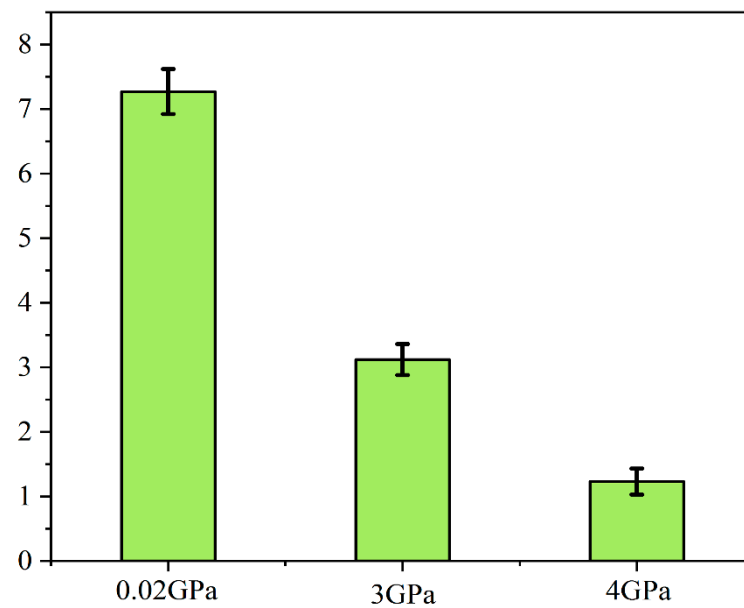


Figure 5. Length-diameter ratio of eutectic Si under different pressures.

The refining process of eutectic Si is mainly affected by nucleation and growth process. Therefore, the influence of pressure on the solidification process can also be considered from these two aspects. On the one hand, pressure affects the nucleation process of eutectic silicon, and its uniform nucleation rate can be expressed as follows [29]:

$$I = I_0 \exp\left(-\frac{\lambda \Delta S_m}{R\tau^2(1-\tau)^3}\right) \exp\left(-\frac{E_0 + \frac{1}{3}V_0P}{RT}\right) = I_0 \exp(-G) \quad (1)$$

where I_0 and λ are constants, ΔS_m is the latent heat of fusion, τ is the relative subcooling, E_0 is the activation energy of crystallization at atmospheric pressure, V_0 is the atomic volume, and G is the activation energy for nucleation. Obviously, the smaller the G , the higher the nucleation rate. Taking its partial derivative with respect to P , we can get:

$$\left(\frac{\partial G}{\partial P}\right)_T = \Delta G \left(5 - \frac{2}{\tau}\right) \frac{1}{T_m} \frac{dT_m}{dP} + \Delta G \frac{1}{\Delta S_m} \frac{d\Delta S_m}{dP} + \frac{1}{3}V_0 \quad (2)$$

Compared with the first two, the last one can be ignored. Therefore, the value of Equation (2) is determined by the first two terms. With the increase of pressure ΔG decreases, which can promote nucleation. In addition, the pressure also has a significant effect on the crystal growth. Under high pressure, the diffusion of atoms will be hindered, and the diffusion activation energy increases, which leads to the decrease of growth rate.

On the other hand, high pressure solidification will lead to the change of solute diffusion coefficient, which will affect the solute redistribution process, change the undercooling degree of solid-liquid interface, and finally affect the solidification microstructure [28].

In conclusion, the microstructure formation mechanism of high pressure solidified $\text{Al}_2\text{O}_3/\text{Al-20Si}$ composite can be revealed in Figure 6, in which magenta, green and white indicate three different crystallization temperatures, namely liquidus temperature, eutectic point temperature and completely solidification temperature. Under the condition of 0.02 GPa, when the temperature is below the liquidus, the black primary silicon begins to nucleate and grow. When the temperature is below the eutectic temperature, eutectic transformation occurs to form $\alpha\text{-Al}$ and eutectic silicon phases. The Yellow alumina phase is dispersed. This may be since Al_2O_3 was used as nucleation substrate for both primary silicon and eutectic silicon. At high pressure, the agglomeration of Al_2O_3 strengthening phase first appeared and gradually disappeared. At the same time, the growth of primary silicon was inhibited, while the nucleation and growth of $\alpha\text{-Al}$ phase were promoted. The eutectic silicon is spheroidized and uniformly distributed under pressure.

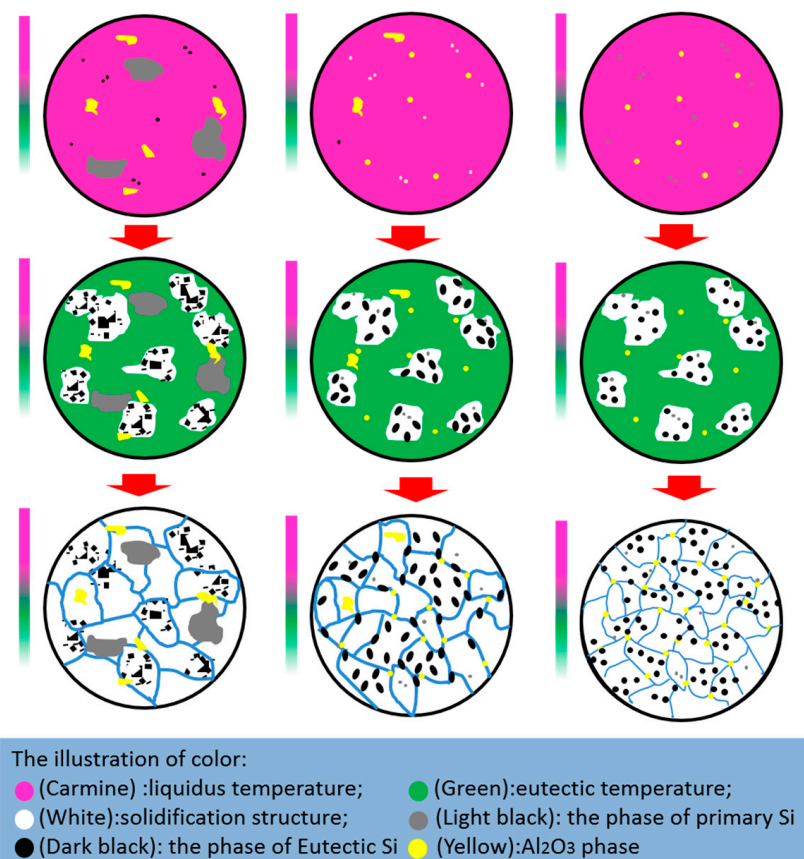


Figure 6. The microstructure formation mechanism of high pressure solidified $\text{Al}_2\text{O}_3/\text{Al-20Si}$ composite.

3.2. Properties of $\text{Al}_2\text{O}_3/\text{Al-20Si}$ Composites

3.2.1. Density of Composite

The density of $\text{Al}_2\text{O}_3/\text{Al-20Si}$ composites prepared by different methods was measured and calculated by Archimedes drainage method as can be seen in Table 2. The results show that the measured density of $\text{Al}_2\text{O}_3/\text{Al-20Si}$ composite prepared by 0.02 GPa is

only 2.52 g/cm³. When solidified at 4 GPa, the measured density increases to 2.78 g/cm³. Compared with high pressure, the pressure 0.02 GPa is lower, which leads to poor fluidity of powder and weak ability of filling voids. Moreover, the wettability of Al₂O₃ and Al-20Si matrix is poor, lead to the exist of interface voids, which will also reduce the density of materials.

Table 2. Density of Al₂O₃/Al-20Si composite.

Pressure	0.02 GPa	3 GPa	4 GPa
Density (g/cm ³)	2.52	2.63	2.78

3.2.2. Microhardness of Composite

The microhardness of Al₂O₃/Al-20Si composite prepared under different pressures is tested. In order to decrease the discrepancy, 5 points are selected for each sample and the average value is taken. The results show that the microhardness of the samples prepared at 0.02 GPa, 3 GPa and 4 GPa are 90.8 HV_{0.05}, 142.6 HV_{0.05} and 156.4 HV_{0.05}, respectively. The reason is that under high pressure, the microstructure is refined, the size of brittle silicon decreases, and the solid solubility of Si in α -Al matrix increases, which results in lattice distortion and hinders the movement of dislocations.

3.2.3. Compressive Strength of Composite

Figure 7 shows the compressive stress-strain curves of Al₂O₃/Al-20Si composites prepared under different pressures. The results show that the strength prepared at 0.02 GPa is 381.5 MPa and the plastic toughness is about 1%. When the solidification pressure is 3 GPa, the compressive strength of the material reaches 451.5 MPa and the compressive strain is about 21%. When the pressure is 4 GPa, the compressive strength of the material is further improved to 469.1 MPa, and the compressive strain is about 21.5%. The compressive strength of the material under high pressure increased by 18% and 23%, respectively. The plasticity increases about 20 times. It is due to the uneven dispersion of the powder under low pressure, resulting in more pores, which seriously affects the density of the composite. At the same time, it cannot prevent the formation of hard brittle primary silicon phase and promote the spheroidization of eutectic silicon under ambient pressure.

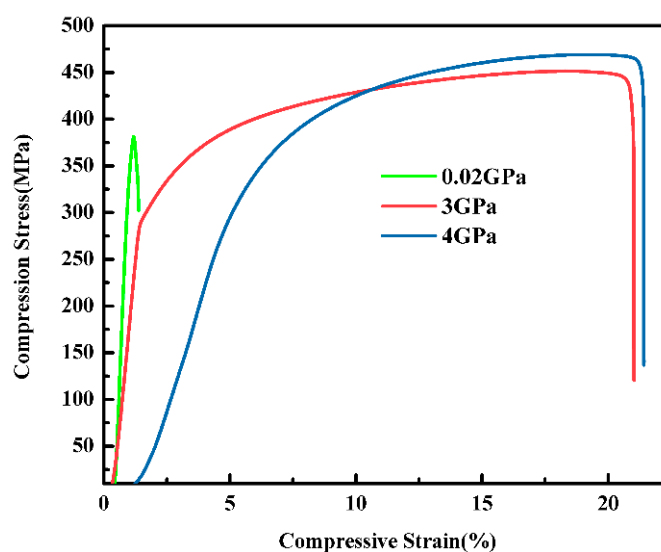


Figure 7. Composite compressive of Al₂O₃/Al-20Si composite.

3.2.4. Fracture Mechanism of Al₂O₃/Al-20Si Composites

The fracture morphology of Al₂O₃/Al-20Si composites under different pressures is shown in Figure 8. It can be seen from Figure 8a that the fracture mode of the alloy during

solidification at 0.02 GPa is typical cleavage fracture, a large number of smooth cleavage planes are distributed in the fracture surface. When the solidification pressure rises to 3 GPa, as shown in Figure 8b, the fracture mode is still cleavage fracture, but its degree decreases. There is no large cleavage plane on the fracture surface, and a small number of dimples have appeared. When the solidification pressure further rises to 4 GPa, as shown in Figure 8c, it can be seen that the fracture mechanism has undergone essential changes, with a large number of dimples distributed on the fracture surface, indicating that the fracture mode of the alloy is quasi-cleavage fracture.

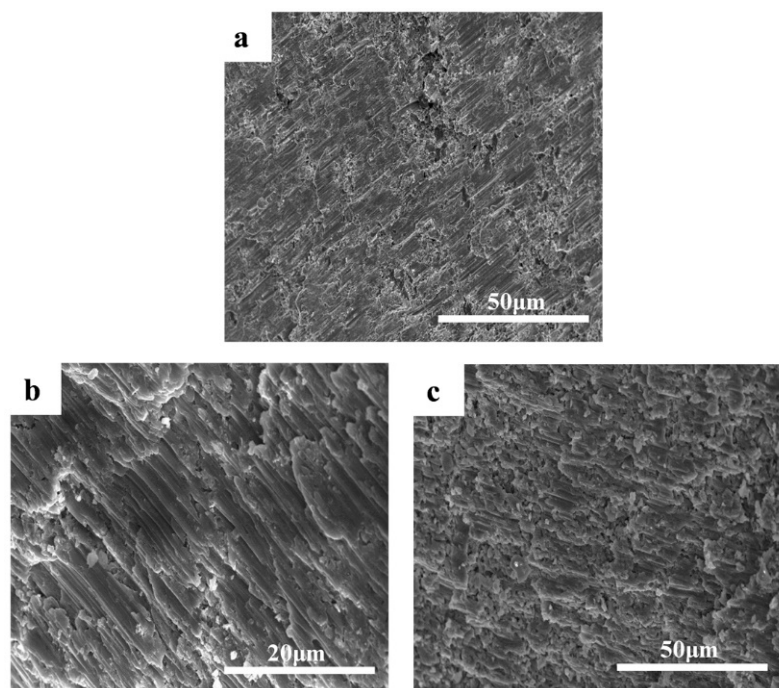


Figure 8. Fracture morphology of $\text{Al}_2\text{O}_3/\text{Al-20Si}$ composites under different pressures (a) 0.02 GPa; (b) 3 GPa; (c) 4 GPa.

4. Conclusions

The microstructure and mechanical properties of $\text{Al}_2\text{O}_3/\text{Al-20Si}$ composites solidified under different pressures were studied. The following conclusions can be drawn:

(1) At 0.02 GPa, primary Si is bulk and contains edges and corners. Under high pressure, the primary Si is greatly inhibited, and with the increase of pressure eutectic Si gradually spheroidized.

(2) Under high pressure, the solid solubility of Si in α phase increases gradually. The solid solubility of Si in α phase increases from 1.94% at 0.02 GPa to 3.94% at 4 GPa, and the solid solubility increases by about 103.1%;

(3) The microhardness of $\text{Al}_2\text{O}_3/\text{Al-20Si}$ composites increased from 102.5 $\text{HV}_{0.05}$ at 0.02 GPa to 156.4 $\text{HV}_{0.05}$ at 4 GPa, which increased by 52.6%. The compressive strength increased from 381.5 MPa at 0.02 GPa to 469.1 MPa at 4 GPa, increasing by 23%.

(4) With the increase of solidification pressure, the fracture mechanism changes from cleavage fracture to quasi cleavage fracture.

Author Contributions: Conceptualization, X.W., Z.C. and T.M.; methodology X.W. and D.Z.; formal analysis D.Z. and T.M.; investigation X.W. and D.D.; resources D.Z.; data curation X.W.; software L.L.; writing—original draft preparation, X.W. and Z.C.; writing—review and editing, D.Z.; X.Y. and G.W. All authors have read and agreed to the published version of the manuscript.

Funding: This work was supported by the Zhejiang Province Natural Science Foundation of China (Grant No.: LQ20E010003, LY18E010003) and the National Natural Science Foundation of China [Nos. 52071165, 52071188, 51801112, 52001262, U1537201, 51501100].

Data Availability Statement: No data, models, or code were generated or used during the study (e.g., opinion or dataless paper).

Conflicts of Interest: The authors declare no conflict of interest.

References

1. Wei, Z.J.; Ma, P.; Wang, H.W.; Zou, C.M.; Scudino, S.; Song, K.; Prashanth, K.G. The thermal expansion behaviour of SiCp / Al–20Si composites solidified under high pressures. *Mater. Des.* **2015**, *65*, 387–394. [[CrossRef](#)]
2. Zeng, J.; Zhu, C.Y.; Wang, W.L.; Li, X.; Li, H.L. Evolution of primary Si phase, surface roughness and mechanical properties of hypereutectic Al–Si alloys with different Si contents and cooling rates. *Phi. Mag. Lett.* **2020**, *100*, 581–587. [[CrossRef](#)]
3. Li, M.J.; Omura, N.; Murakami, Y.; Matsui, I.; Tada, S. A comparative study of the primary phase formation in Al–7 wt% Si and Al–17 wt% Si alloys solidified by electromagnetic stirring processing. *Mater. Today Commun.* **2020**, *24*, 101146. [[CrossRef](#)]
4. Langelandsvi, K.G.; Horgar, A.; Furu, T.; Roven, H.J.; Akselsen, O.M. Comparative study of eutectic Al–Si alloys manufactured by WAAM and casting. *Int. J. Adv. Manuf.* **2020**, *110*, 935–947. [[CrossRef](#)]
5. Zhang, B.; Zhao, Y.H.; Wang, H.; Chen, W.P.; Hou, H. Three-Dimensional Phase Field Simulation of Dendritic Morphology of Al–Si Alloy. *Rare Met. Mater. Eng.* **2019**, *48*, 2835–2840.
6. Zhang, H.T.; Zuo, K.S.; Han, X. Effects of P+Cr complex modification and solidification conditions on microstructure of hypereutectic Al–Si alloys by wedge-shaped copper mould casting. *China Foundry* **2014**, *11*, 481–486.
7. Chen, C.; Liu, Z.X.; Ren, B.; Wang, M.X.; Weng, Y.G.; Liu, Z.Y. Influences of complex modification of P and RE on microstructure and mechanical properties of hypereutectic Al–20Si alloy. *Nonferr. Met. Soc.* **2007**, *17*, 301–306. [[CrossRef](#)]
8. Xu, C.L.; Jiang, Q.C.; Yang, Y.F.; Wang, H.Y.; Wang, J.G. Effect of Nd on primary silicon and eutectic silicon in hypereutectic Al–Si alloy. *J. Alloys Compd.* **2006**, *422*, L1–L4. [[CrossRef](#)]
9. Barrirero, J.; Li, J.H.; Engstler, M.; Ghafoor, N.; Schumacher, P.; Oden, M.; Mucklich, F. Cluster formation at the Si/liquid interface in Sr and Na modified Al–Si alloys. *Scripta Mater.* **2016**, *117*, 16–19. [[CrossRef](#)]
10. Wei, H.M.; Geng, L.; Zhang, X.X. Solidification behavior of SiCw / Al–18Si composites, *Rare Met.* **2007**, *26*, 237–241. *Rare Met.* **2007**, *26*, 237–241.
11. Lien, H.H.; Mazumder, J.; Wang, J.; Misra, A. Ultrahigh strength and plasticity in laser rapid solidified Al–Si nanoscale eutectics. *Mater. Res. Lett.* **2020**, *8*, 291–298. [[CrossRef](#)]
12. Tian, J.T.; Piñero, E.; Narciso, J.; Louis, E. Effects of temperature on pressure infiltration of liquid Al and Al–12 wt.% Si alloy into packed SiC particles. *Scripta Mater.* **2005**, *53*, 1483–1488. [[CrossRef](#)]
13. Yan, W.; Chen, W.Q.; Zhang, S.L.; Li, B.; Li, J. Evolution of solidification structures and mechanical properties of high-Si Al alloys under permanent magnetic stirring. *Mater. Charact.* **2019**, *157*, 109894. [[CrossRef](#)]
14. Haghayeghi, R.; de Paula, L.C.; Zoqui, E.J. Comparison of Si Refinement Efficiency of Electromagnetic Stirring and Ultrasonic Treatment for a Hypereutectic Al–Si Alloy. *J. Mater. Eng. Perform.* **2017**, *26*, 1900–1907. [[CrossRef](#)]
15. Selivorstov, V.; Dotsenko, Y.; Borodianskiy, K. Influence of Low-Frequency Vibration and Modification on Solidification and Mechanical Properties of Al–Si Casting Alloy. *Materials* **2017**, *10*, 560. [[CrossRef](#)]
16. Choi, H.; Konishi, H.; Li, X. Al₂O₃ nanoparticles induced simultaneous refinement and modification of primary and eutectic Si particles in hypereutectic Al–20Si alloy. *Mater. Sci. Eng. A* **2012**, *541*, 159–165. [[CrossRef](#)]
17. Li, Q.; Xia, T.; Lan, Y.; Zhao, W.; Fan, L.; Li, P. Effect of in situ γ -Al₂O₃ particles on the microstructure of hypereutectic Al–20%Si alloy. *J. Alloys Compd.* **2013**, *577*, 232–236. [[CrossRef](#)]
18. Megahed, M.; Saber, D.; Agwa, M.A. Modeling of Wear Behavior of Al–Si / Al₂O₃ Metal Matrix Composites. *Phys. Met. Metallogr.* **2019**, *120*, 981–988. [[CrossRef](#)]
19. Choi, H.; Li, X. Refinement of primary Si and modification of eutectic Si for enhanced ductility of hypereutectic Al–20Si–4.5Cu alloy with addition of Al₂O₃ nanoparticles. *J. Mater. Sci.* **2012**, *47*, 3096–3102. [[CrossRef](#)]
20. Bramfitt, B.L. The effect of carbide and nitride additions on the heterogeneous nucleation behavior of liquid iron. *Metall. Trans.* **1970**, *1*, 1987–1995.
21. Wang, X.H.; Ran, Z.; Wei, Z.J.; Zou, C.M.; Wang, H.W.; Gouchi, J.; Uwatoko, Y. The formation of Bulk β -Al₃Ni phase in eutectic Al–5.69wt%Ni solidified under high pressure. *J. Alloys Compd.* **2017**, *42*, 670–675. [[CrossRef](#)]
22. Wang, X.H.; Wang, H.W.; Zou, C.M.; Wei, Z.J.; Uwatoko, Y.; Gouchi, J. The effect of high pressure and superheating and superheating on the planar growth of Al₃Ni phase in hypo-peritectic Al–30wt%Ni alloy. *J. Alloys Compd.* **2019**, *772*, 1052–1060. [[CrossRef](#)]
23. Wang, X.H.; Wang, H.W.; Wei, Z.J.; Zou, C.M. Al₃Ni alloy synthesized at high pressure and its Debye temperature. *J. Alloys Compd.* **2019**, *774*, 364–369. [[CrossRef](#)]
24. Zhu, D.D.; Dong, D.; He, Q.; Zhou, Z.Z.; Zhang, Y.X.; Wang, Q.B.; Ni, C.Y. Instability mechanism of lamellar structures of Ti–48Al alloy solidified under high pressure. *Rare Met. Mater. Eng.* **2017**, *46*, 217–220.
25. Ma, P.; Zou, C.M.; Wang, H.W.; Scudino, S.; Fu, B.G.; Wei, Z.J.; Kuhn, U.; Eckert, J. Effects of high pressure and SiC content on microstructure and precipitation kinetics of Al–20Si alloy. *J. Alloys Compd.* **2014**, *586*, 639–644. [[CrossRef](#)]
26. Lin, X.P.; Fan, Z.B.; Xu, C.; Yuo, G.K.; Guo, S.Q. Room temperature compressive properties and strengthening mechanism of Mg96.17Zn3.15Y0.50Zr0.18 alloy solidified under high pressure. *J. Rare Earths* **2020**, *38*, 657–664. [[CrossRef](#)]

-
27. Liu, X.; Ma, P.; Jia, Y.D.; Wei, Z.J.; Suo, C.J.; Ji, P.C.; Shi, X.R.; Yu, Z.S.; Prashanth, G.K. Solidification of Al-xCu alloy under high pressures. *J. Mater. Res. Technol.* **2020**, *9*, 2983–2991. [[CrossRef](#)]
 28. Batashef, A.E. *Crystallization of Metals and Alloys at Pressure*, 1st ed.; Moscow Metallurgy: Moscow, Russia, 1977.
 29. Thompson, C.V.; Spaepen, F. Homogeneous crystal nucleation in binary metallic melts. *Acta Met.* **1983**, *31*, 2021–2027. [[CrossRef](#)]